

Nitride Wide-Bandgap Semiconductors for UV Nonlinear Optics

Shihang Li ^{1,2} and Lei Kang ^{1,*} 

¹ Functional Crystals Lab, Key Laboratory of Functional Crystals and Laser Technology, Technical Institute of Physics and Chemistry, Chinese Academy of Sciences, Beijing 100190, China

² University of Chinese Academy of Sciences, Beijing 100049, China

* Correspondence: kanglei@mail.ipc.ac.cn

Abstract: Nitride wide-bandgap semiconductors possess a wide tunable energy bandgap and abundant coordination anionic groups. This suggests their potential to display nonlinear optical (NLO) properties in the UV wavelength spectrum. This paper reports recent progress and material discoveries in exploring UV NLO structures using nitrides. The study emphasizes their underlying structure–property correlations in order to provide a summary of the potential performance and application value of important nitride NLO crystals. Additionally, the text underscores the benefits of nitrides in terms of optical transparency, second-harmonic-generation effects, and the birefringent phase matching output wavelength limits, while addressing current issues in terms of theoretical outlook and experimental exploration.

Keywords: nitride; ultraviolet; nonlinear optical crystal; first-principles calculation

1. Introduction

Nitrides are significant wide-bandgap semiconductor materials with a variety of optoelectronic applications in different fields of electronic devices, such as high-voltage devices, solar-blind photodetectors, and waveguide devices [1]. Their excellent physical–chemical properties and tunable energy bandgap (E_g) over a wide range make them ideal for these applications. Typical wide-bandgap nitride semiconductors include the third-generation semiconductor GaN [2], ultraviolet (UV) light-emitting material AlN [3] or its solid-solution structure (Ga,Al)N [4], graphene-like layered material h-BN [5], and ceramic material Si_3N_4 [6]. The wide-bandgap E_g rendered the aforementioned materials naturally suitable for use in optoelectronic applications and the study of light–matter interaction in the UV band (100–400 nm). The UV band is typically divided into three segments: UVA (320–400 nm long-wave UV), UVB (280–320 nm mid-wave UV), and UVC (100–280 nm short-wave UV). UVC, in turn, is divided into 200–280 nm solar-blind UV and 100–200 nm deep-UV light [7].

The UV laser is a cutting-edge high-tech solution for UV optoelectronic applications that has added significant value in many areas, including spectroscopy, medicine, and photolithography [8–11]. One main technical route in UV laser production involves converting traditional micrometer lasers, such as the Nd: YAG 1064 nm laser [12], into UV lasers using the cascade harmonic generation effect of nonlinear optical (NLO) crystals. This typically involves generating 355 nm for the third harmonic generation, 266 nm for the fourth harmonic generation, and 177 nm for sixth harmonic generation based on the fundamental wavelength of 1064 nm [13]. NLO crystals serve as the irreplaceable functional material basis for laser generation, especially for the two crucial solar-blind UV and deep-UV bands. However, the need for NLO performance has increased as second-harmonic-generation (SHG) wavelengths shift to short-wave UV light, posing a challenge in crystal selection [14]. Apart from broad UVC transparency induced by a wide-bandgap E_g , the crucial phase-matching (PM) performance is indispensable [15,16]. Regrettably, the availability of NLO crystals that satisfy the optimal frequency conversion for solar-blind 266 nm and deep-UV



Citation: Li, S.; Kang, L. Nitride Wide-Bandgap Semiconductors for UV Nonlinear Optics. *Crystals* **2023**, *13*, 1536. <https://doi.org/10.3390/cryst13111536>

Academic Editors: Lin Xiong, Liujiang Zhou and Sumit Mazumdar

Received: 30 August 2023

Revised: 20 September 2023

Accepted: 24 September 2023

Published: 26 October 2023



Copyright: © 2023 by the authors. Licensee MDPI, Basel, Switzerland. This article is an open access article distributed under the terms and conditions of the Creative Commons Attribution (CC BY) license (<https://creativecommons.org/licenses/by/4.0/>).

177 nm is limited. The development of UVC laser technology has been limited by the search for NLO crystals that are appropriate for the UVC band.

Traditionally, UV NLO crystal research has focused on phosphates and borates such as KH_2PO_4 (KDP) [17], LiB_3O_5 (LBO) [18], $\beta\text{-BaB}_2\text{O}_4$ (BBO) [19], and $\text{KBe}_2\text{BO}_3\text{F}_2$ (KBBF) [20]. There has been a recent surge in the exploration of UV NLO materials derived from carbonates, nitrates, and sulfates [21–23]. Compared to these traditional and emerging UV NLO systems, NLO nitride research has also made significant progress in recent years. This mainly includes the CN-based NLO system [24], PN-based NLO system [25], and SiN-based NLO system [26], which has a larger bandgap E_g than GaN (~3.4 eV), as well as other nitrides such as Zn_2NCl [27] and NaSnN [28], the latter having a smaller bandgap E_g than GaN. These NLO nitrides show a variety of anionic group structures and structure–property relationships [29–34]. Encouragingly, the output wavelengths of their phase-matching SHG can span the UV spectrum and even extend into the deep-UV bands. Therefore, this study focuses on the research progress of nitrides in UV nonlinear optics, which is of great practical significance for comprehensively discussing their NLO structure–property relationships in the UVC region. It also serves as a catalyst for sorting out the development and experimental exploration of this system.

2. Methods

With the advancement of high-performance computing, first-principles calculations offer significant advantages for the assessment of mechanical, thermal, optical, and electrical properties of functional crystals. In evaluating crucial NLO properties, like refractive indices, birefringence, energy bandgap, and effective SHG coefficients, first-principles calculations furnish efficient and effective computational and analytical methods and solutions for material design [35]. Given the scarcity of reports on nitride NLO crystals and the challenging conditions of nitride crystal growth, the initial assessment made using first-principles calculations holds promise for evaluating overall performance and comprehensively directing the use of nitrides. This approach can effectively prevent aimless and time-consuming compound exploration and experimental characterization [36]. The information in this study is primarily obtained from first-principles calculations found in the existing literature. Notably, the calculated results on the linear and NLO properties for the benchmark materials GaN and Si_3N_4 in the nitride system exhibit remarkable accuracy [26,30], supporting the reasonableness and dependability of the theoretical studies for use clarifying structure–property correlations and anticipating new materials. In this paper, to enhance the lucidity of the structure–property evolutions, we include additional data while maintaining computational parameters' consistency.

3. Results

Note that nitrogen (N) is only less electronegative than fluorine (F) and oxygen (O), similar to chlorine (Cl). Therefore, the relatively weak coupling strength of covalent nitride bonds may lead to a small gap developing between the highest occupied molecular orbitals (HOMO) and the lowest unoccupied molecular orbitals (LUMO). In other words, the energy bandgaps (E_g) of nitrides are typically slightly lower than those of fluorides or oxides. However, nitrides can also be bonded by the continued oxidation of F or O, resulting in the potential creation of fluoronitrides or oxynitrides. These fluoronitride or oxynitride compounds can further increase the energy bandgap E_g , making them appropriate for wider optical transparency at shorter UV wavelengths. It should be emphasized that the NLO effects and birefringence are frequently linked with covalent anionic motifs. Additionally, it should be noted that the coordination motifs of nitrogen, similar to those of oxygen, can also exhibit a broad range of anionic groups due to the variety of central cationic coordination bonds and skeletal arrangements. The quantity of noncentrosymmetric nitride structures in the inorganic crystal structure database (ICSD) is comparatively substantial. These structures feature various central cationic covalent motifs and showcase a broad selection of dimensional configurations, as well as coordinating group structures that

incorporate oxygen or halogen. In addition, these structures contain ligand oxygen or halogen radical structures. Here, we adhere to the principle of bandgap-first screening, focusing on the nitride structures with wide UVC bandgaps ($E_g > 4.4$ eV, $\lambda_{UV} < 280$ nm) and large birefringence ($\Delta n > 0.05$). These structures are more likely to achieve a phase-matching SHG output $\lambda_{PM} < 280$ nm in the UVC region. Their crystal and motif structures are presented in Figure 1. Meanwhile, Table 1 provides details on their energy bandgaps E_g , SHG coefficients d_{ij} , birefringence Δn , UV absorption edges λ_{UV} , and phase-matching SHG limits λ_{PM} in comparison with the $\text{CO}(\text{NH}_2)_2$ (urea) crystal [37] containing typical N-H bonds, GaN, AlN, and Si_3N_4 as the benchmark wide-bandgap nitride semiconductors. We will now classify the structure–property relationships of NLO nitrides using various motifs based on Figure 1 and Table 1.

3.1. GaN and AlN with Tetrahedral $[\text{GaN}_4]$ or $[\text{AlN}_4]$ Motif

Group IIIA nitrides are vital semiconductor materials and they have become the most valuable semiconductor alloy system for short-wavelength light-emitting diodes (LEDs) and laser development, with various applications. The synthesis of binary and ternary nitrides of group IIIA has been critical in the growth of gas phase chemical vapor deposition (CVD) techniques [38]. For instance, the growth conditions in $\text{Al}_{0.85}\text{Ga}_{0.15}\text{N}$ were adjusted via the use of a hot-wall MOCVD system to decrease the compensation of native defects, resulting in an elevation of p-type conductivity [39].

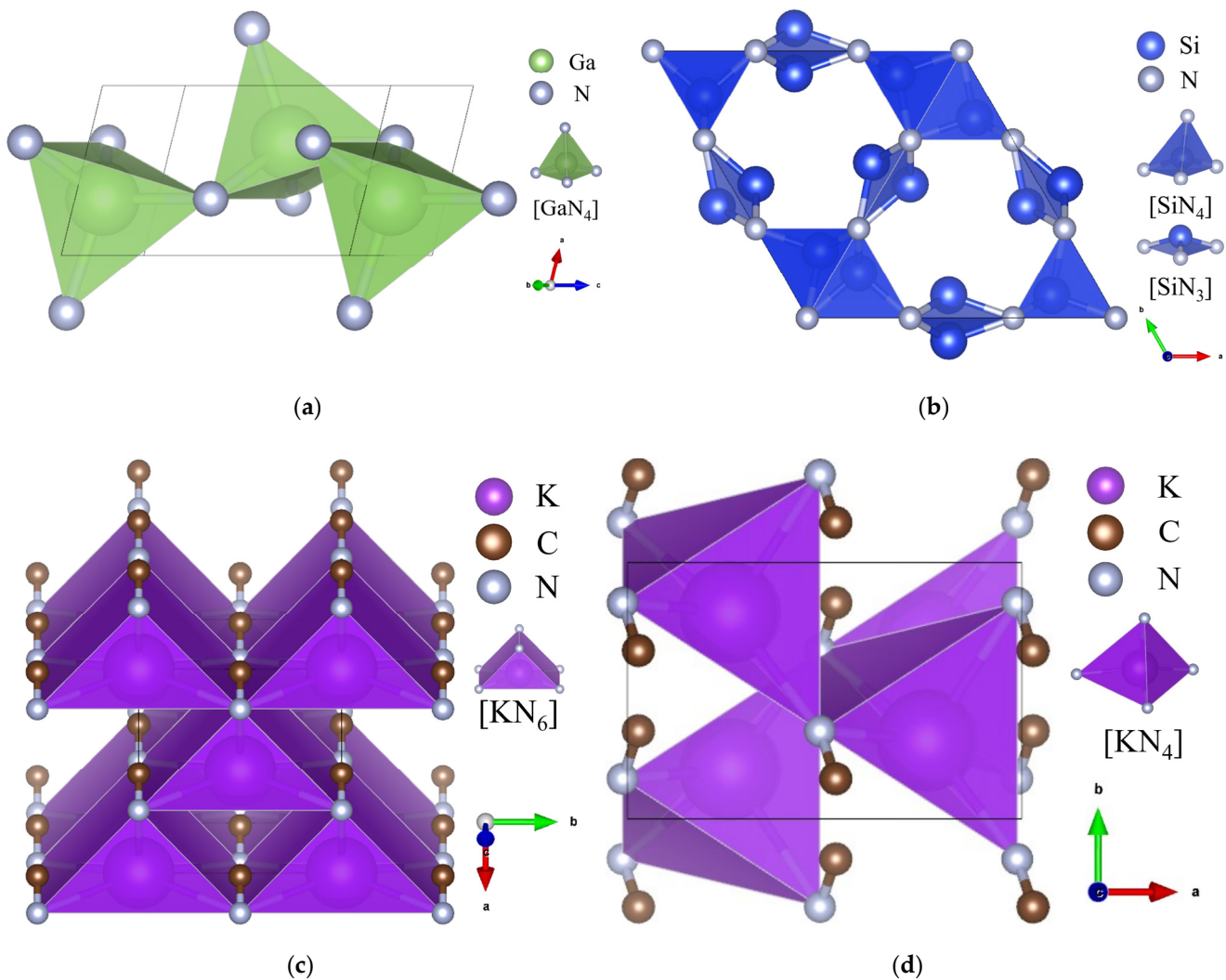
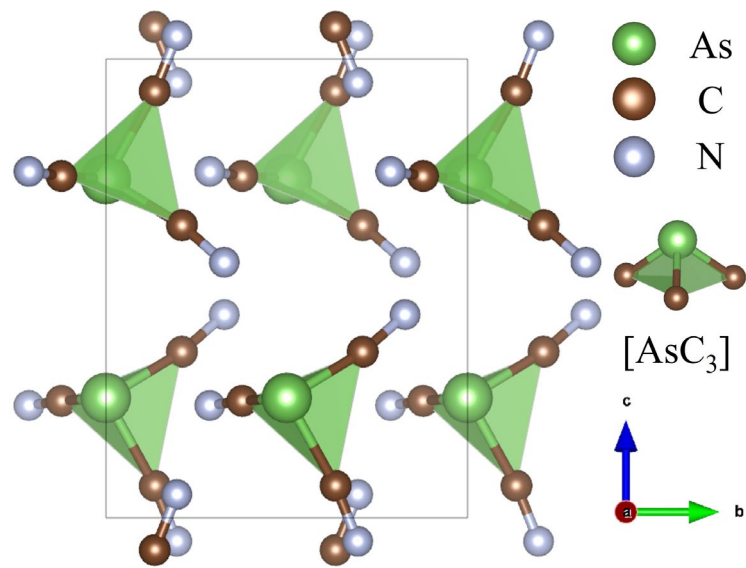
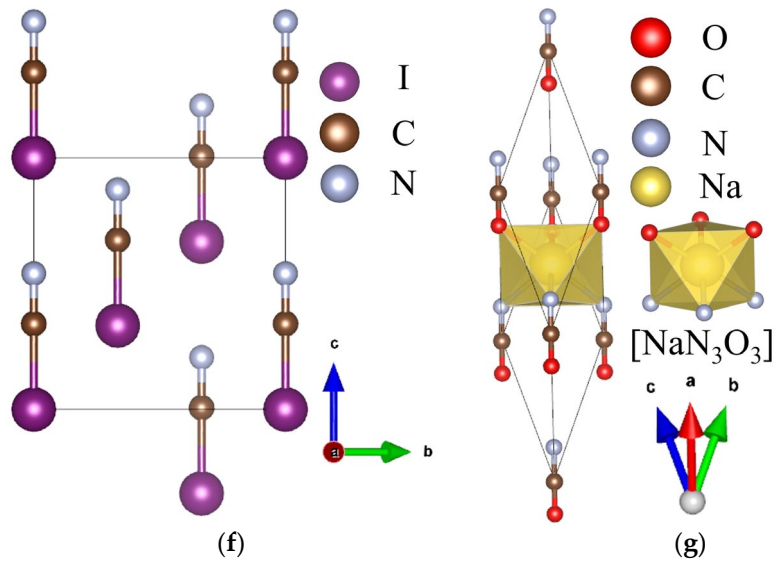


Figure 1. Cont.

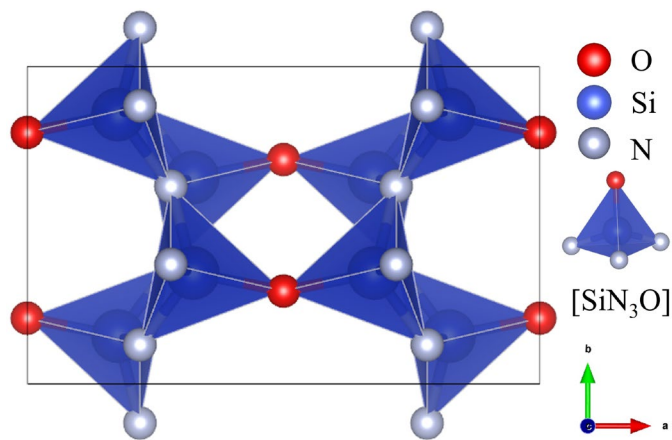


(e)



(f)

(g)



(h)

Figure 1. Cont.

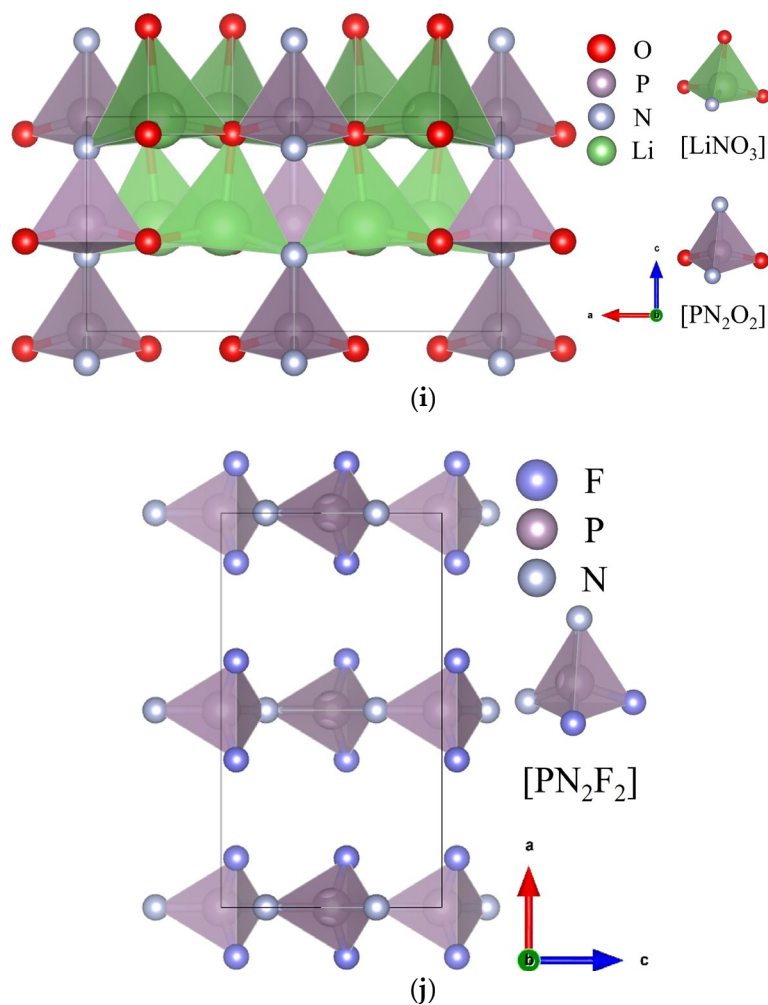


Figure 1. Crystal and motif structures of GaN or AlN (a), Si₃N₄ (b), α-KCN (c), β-KCN (d), AsC₃N₃ (e), CNI (f), NaCNO (g), Si₂N₂O (h), Li₂PNO₂ (i), and PNF₂ (j). In the legends, *a*, *b*, and *c* indicate the orientation of the crystal axis.

Table 1. Energy bandgaps E_g , SHG coefficients d_{ij} , birefringence Δn , UV absorption edges λ_{UV} , and phase-matching SHG limits λ_{PM} of typical wide-bandgap NLO nitrides.

	Symmetry	Motifs	E_g (eV)	d_{ij} (pm/V)	$ \Delta n @$ 1064 nm	λ_{UV} (nm)	λ_{PM} (nm)	Refs.
CO(NH ₂) ₂	P-4 ₂₁ m	Cal.	6.35	$d_{36} = 1.70$	0.111	195	245	[37]
		Exp.	6.18	$d_{36} = 1.30$	0.102	201	---	[24]
GaN	P6 ₃ mc	[GaN ₄]	3.50	$d_{31} = 2.42; d_{33} = -3.64$	0.017	354	---	[30]
AlN	P6 ₃ mc	[AlN ₄]	6.20	$d_{31} = 0.23; d_{33} = 0.86$	0.023	200	---	[30]
α-KCN	Cm	[CN]	7.11	$d_{15} = 0.76$	0.117	175	198	[24]
β-KCN	Cc	[CN]	7.60	$d_{11} = 0.59$	0.121	164	180	[24]
AsC ₃ N ₃	C ₂	[CN] + [AsC ₃]	5.96	$d_{22} = 0.71$	0.123	208	235	[24]
CNI	R ₃ m	[CNI]	5.34	$d_{33} = 16.95$	0.737	233	233	[24]
NaCNO	R ₃ m	[CNO]	5.20	$d_{33} = 0.66$	0.374	239	239	[24]
α-Si ₃ N ₄	P3 ₁ c	[SiN ₄]	4.60	$d_{15} = 0.50; d_{24} = 0.50$	0.016	270	---	[26]
Si ₂ N ₂ O	CmC ₂₁	[SiN ₃ O]	5.00	$d_{24} = 1.00; d_{33} = -0.86$	0.080	249	285	[26]
Li ₂ PNO ₂	CmC ₂₁	[PN ₂ O ₂]	6.98	$d_{32} = 0.79; d_{33} = -0.95$	0.067	178	264	[25]
PNF ₂	CmC ₂₁	[PN ₂ F ₂]	8.80	$d_{32} = 0.44; d_{33} = -0.86$	0.164	142	142	[25]

“---” equals no suitable data.

GaN is a third-generation semiconductor with a wide bandgap $E_g \sim 3.5$ eV [30]. However, its tetrahedral $[\text{GaN}_4]$ framework structure (see Figure 1a) results in relatively low structural anisotropy and a small birefringence Δn of only 0.017 (see Table 1). Therefore, it cannot meet the requirements for conventional birefringent phase matching in the UV region. AlN, which has the same structure, faces a similar problem. Despite its large bandgap E_g of 6.2 eV [30], the value of birefringence Δn is still small, being only ~ 0.023 , and the material does not have sufficient ability for birefringent phase matching in the UV region. Although it is feasible to develop GaAlN solid solutions with a tunable bandgap E_g , birefringent properties are linked to the local structural anisotropy with minimal improvement. Consequently, such solid solutions remain largely incapable of producing a coherent phase-matching SHG output, especially in the UVC band. This scenario can be observed in $\alpha\text{-Si}_3\text{N}_4$ with the tetrahedral $[\text{SiN}_4]$ motif (see Figure 1b).

3.2. KCN and AsC_3N_3 with Chained [CN] Motif

An effective scheme to increase the birefringence Δn is to increase the structural anisotropy of the anionic motif. The chain-like [CN] motif is a potential nitride birefringent anionic motif. In a typical KCN compound [24], the CN triple bond determines the bandgap E_g required to reach deep-UV light ($E_g \sim 7.1$ eV for $\alpha\text{-KCN}$ and 7.6 eV for $\beta\text{-KCN}$). The difference in K coordination slightly raises the bandgap E_g from $\alpha\text{-KCN}$ with four coordinations (see Figure 1c) to $\beta\text{-KCN}$ with six coordinations (see Figure 1d). Despite the staggered arrangement of isolated [CN] motifs, the resulting SHG effects ($d_{15} = 0.76$ pm/V for $\alpha\text{-KCN}$ and $d_{11} = 0.59$ pm/V for $\beta\text{-KCN}$) still exceed those of KDP ($d_{36} = 0.39$ pm/V). Most importantly, their birefringence Δn are both sufficiently large, standing at ~ 0.117 and 0.121, respectively, for $\alpha\text{-KCN}$ and $\beta\text{-KCN}$. Consequently, the $\alpha\text{-KCN}$ and $\beta\text{-KCN}$ crystals can achieve phase-matching SHG output wavelengths of 198 nm and 180 nm, which successfully expand into the deep-UV region. Furthermore, when the pyramid $[\text{AsC}_3]$ motifs with lone-paired electrons (see Figure 1e) are combined with the chained [CN] motifs, the bandgap E_g in the resulting AsC_3N_3 [24] structure is determined by the As-C bond, reducing it to $E_g \sim 6.0$ eV. Unfortunately, because the $[\text{AsC}_3]$ polar motifs are aligned head-to-head, the SHG effect is weakened ($d_{22} = 0.71$ pm/V), although it still in the order of KCN. On the upside, the birefringence Δn is still large enough to achieve a phase-matching SHG output of 235 nm for lasing in the solar-blind UV region using the practical 266 nm laser.

3.3. CNI and NaCNO with Chained [CNI] or [CNO] Motif

The birefringence and SHG effects can be significantly increased through the parallel alignment of the chained [CN] polar motifs. The coordination of isolated [CN] motifs with iodine (I) forms longer chain-like [CNI] dipole molecules (see Figure 1f), which belong to this type of parallelly aligned structure [24]. Consequently, these polar molecule crystals exhibit optimal isotropic alignment with a birefringence Δn of 0.7 and an SHG effect of 16 pm/V. Unfortunately, CNI has a bandgap E_g of ~ 5.3 eV, much smaller than those of KCN, limiting its phase-matching SHG output to only 233 nm, which is insufficient for the deep-UV region, but still sufficient for the solar-blind UV region. Similarly, the [CN] motif in NaCNO coordinates with oxygen (O) to form a [CNO] polar anionic chain (see Figure 1g) with a large birefringence Δn of 0.3, allowing the phase-matching SHG output to reach 239 nm [24]. This performance is also achievable for the solar-blind UV band and superior to the UV NLO performance of the classical urea NLO crystal. However, the intrinsic dipole moment of the [CNO] motif is canceled by C and O at both ends, resulting in an SHG effect of only 0.66 pm/V, which is still larger than that of KDP.

3.4. $\alpha\text{-Si}_3\text{N}_4$ and $\text{Si}_2\text{N}_2\text{O}$ with Tetrahedral $[\text{SiN}_4]$ or $[\text{SiN}_3\text{O}]$ Motif

Another effective way to increase the structural anisotropy of a tetrahedron is by modifying N with O, which alters the difference in bond lengths of regular tetrahedra. For example, transitioning from $\alpha\text{-Si}_3\text{N}_4$ to $\text{Si}_2\text{N}_2\text{O}$, as shown in Figure 1h, elevates the local

anisotropy of the tetrahedral [SiN₃O] structure, raises the birefringence Δn of Si₂N₂O to 0.08 (exp. ~ 0.11), and produces a phase-matching SHG output of 285 nm [26]. Regrettably, the structural anisotropy of Si₂N₂O is still not sufficiently extended, which, together with the insufficiently large bandgap $E_g \sim 5.0$ eV, results in a phase-matching SHG output that does not reach the UVC region. Additionally, the SHG effect (e.g., $d_{24} = 1.0$ pm/V) is almost doubled compared to α -Si₃N₄ (e.g., $d_{24} = 0.5$ pm/V, refer to Table 1) due to the enlarged distortion of the polar tetrahedral framework. It is worth noting that this theoretical prediction has also received preliminary experimental confirmation [26], which somewhat suggests the potential of nitrides as UV NLO materials.

3.5. Li₂PNO₂ and PNF₂ with Poly-Chained [PN₂O₂] or [PN₂F₂] Motif

Similar to [SiN₄], the [PN₄] motif exhibits a small degree of structural anisotropy; nevertheless, the bandgap E_g of the P-N bond is generally larger than that of the Si-N bond. By applying the strategy outlined in Section 3.4 to P-N structures, it may be feasible to extend the UV NLO capacity into the solar-blind UV or even the deep-UV regions. The phosphazene system has been demonstrated to undergo reasonable expansion in this regard [25]. In this case, Li₂PNO₂ alters the [PN] with O, forming a tetrahedral [PN₂O₂] poly-chained arrangement (see Figure 1i). As a result, the birefringence Δn increases to 0.067, enabling phase-matching SHG output at 264 nm in the solar-blind UV region. If the [PN] is further modified to become [PN₂F₂] and arranged in a chain-parallel van der Waals (vdW) polymer structure (see Figure 1j), the resulting birefringence Δn of the PNF₂ structure increases to 0.16. This yields a phase-matching SHG limit of 142 nm, which is shorter than KBBF's 161 nm limit. It is important to emphasize that this meets the requirements for the application of a 150 nm atomic clock [40]. Moreover, these two polar poly-chained structures exhibit relatively large SHG effects twice that of KDP, with ~ 0.95 pm/V for Li₂PNO₂ and 0.86 pm/V for PNF₂, respectively (see Table 1). Meanwhile, the one-dimensional chain-like structure may be useful in fiber-optic devices and deep-UV light guiding and does not require vacuum conditions. All of these results demonstrate the significant potential of the phosphazene structures to perform well in the two critical UVC bands [25].

4. Discussion

In Section 3, we described in detail the five nitride NLO motifs as shown in Figure 1, including the tetrahedral [Ga/AlN₄] motif, chained [CN] motif, chained [CNI] or [CNO] motif, distorted tetrahedral [SiN₃O] motif, and poly-chained [PN₂O₂] or [PN₂F₂] motif. With reference to the first-principles calculation results listed in Table 1, we further elaborated on their UV NLO properties, including energy bandgap, UV absorption edge, birefringence, and phase-matching SHG output wavelength. The origin of these properties is consistent with our analysis of the conformational relationships of the nitride motifs. Next, in order to more visually assess the potential of nitride use in UV NLO materials, we labeled the structures in Table 1 with the UV absorption edges λ_{UV} and labelled those in Figure 2 with phase-matching SHG limits λ_{PM} in the order of wavelength in the electromagnetic spectrum.

It can be summarized that the UV absorption edges λ_{UV} for these typical nitride structures range from 270 nm to 142 nm, while the phase-matching SHG limits λ_{PM} range from 285 nm to 142 nm. This theoretically enables the phase-matching SHG output in the UVC band. Specifically, using two structural design strategies to expand anisotropy, PNF₂, β -KCN, and α -KCN can achieve the shortest phase-matching SHG output wavelengths of 142 nm, 180 nm, and 198 nm in the deep-UV (100 nm to 200 nm) region, respectively. Meanwhile, CNI, AsC₃N₃, NaCNO, and Li₂PNO₂ can achieve the shortest phase-matching SHG output wavelengths of 233 nm, 235 nm, 239 nm, and 264 nm in the solar-blind UV (200 nm to 280 nm) region, respectively. Moreover, these NLO nitrides exhibit a relatively large birefringence and SHG effect compared to traditional NLO oxides. Their birefringence ranges from 0.067 to 0.737, with SHG effects that are typically greater than those of KDP.

In some cases (e.g., CNI), the SHG effect even reaches the order of the infrared NLO benchmark material AgGaS_2 ($d_{36} = 13 \text{ pm/V}$). These findings demonstrate the considerable potential of nitride use in UV nonlinear optics.

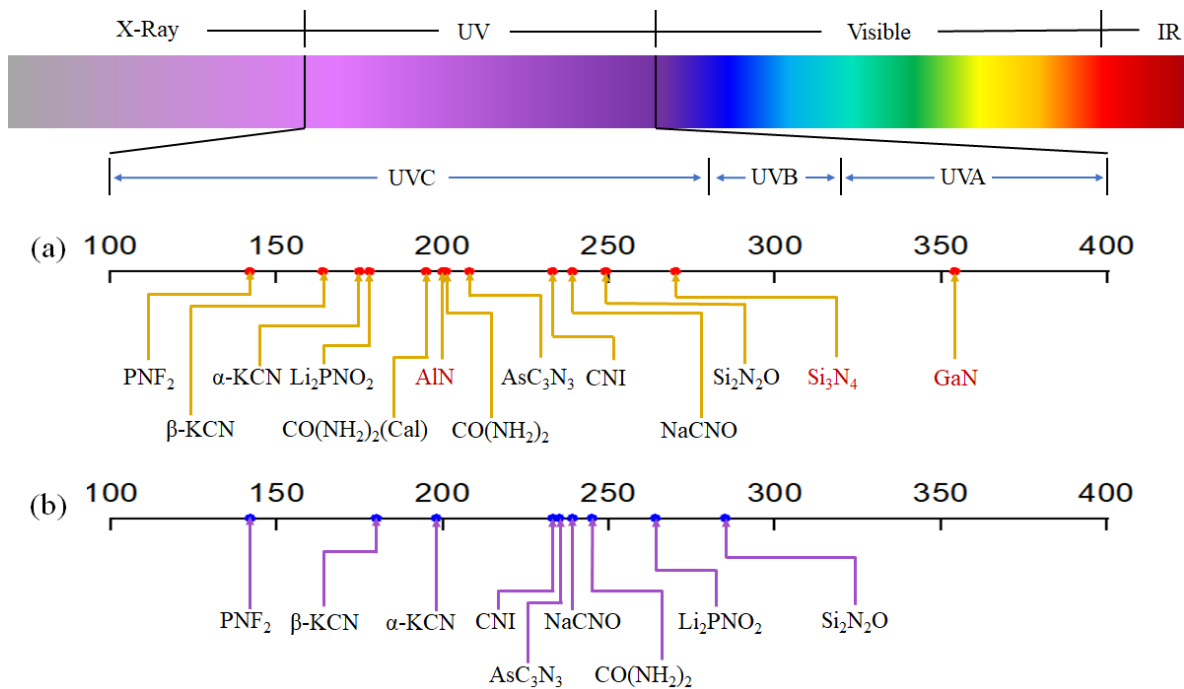


Figure 2. UV absorption edges λ_{UV} (a) and phase-matching SHG limits λ_{PM} (b) of the NLO structures in Table 1 across the electromagnetic spectrum. GaN , AlN , and Si_3N_4 are listed as comparisons.

In fact, the benefits of nitrides can also be achieved through the nitrogen (N) substitution of oxygen (O) in oxides. This is evidenced by examples such as $\text{M}(\text{NH}_2\text{SO}_3)_2$ ($\text{M} = \text{Sr}, \text{Ba}$) with $[\text{SO}_3\text{N}]$ motif [41] and NaPO_3NH_3 with the $[\text{PO}_3\text{N}]$ motif [42]. This avenue of exploration should also be considered in the development of UV NLO structures for oxynitrides. However, the experimental exploration of nitrides, especially inorganic nitride NLO materials, is usually more difficult than that of oxides because of the need for an oxygen-free experimental environment. Even if some oxynitrides (e.g., $\text{Si}_2\text{N}_2\text{O}$) can be synthesized under laboratory conditions, their large-sized single-crystal growth faces many challenges, including in terms of structural stability and crystal defects. Therefore, the exploration of nitride NLO materials still requires the tireless efforts of experimental scientists.

The thermal stability of wide-bandgap nitride materials, in addition to their NLO properties, significantly impacts their applications. To evaluate the thermal stability, one can resort to first-principles calculations. A first-principles-based synthetic growth concept was utilized to investigate the formation mechanism of self-induced InAlN core-shell nanorods (NRs) to address precursor prevalence and energetics [43]. We contend that the advancement of this field will be augmented through the utilization of first-principles design and simulation.

5. Evaluation and Outlook

The exploration of UV NLO materials has predominantly focused on oxides, while IR NLO materials have been chiefly pursued in sulfur and phosphorus compounds. Nonetheless, the potential benefits of investigating NLO materials within nitride systems remain largely untapped although the attention paid to polarity in other fields [44–48]. This article highlights the importance of using nitride NLO materials to achieve optical frequency conversion in UV and deep-UV regions. It does so by conducting a thorough evaluation of the linear and NLO properties present in wide-bandgap nitride material systems. This paper presents an approach for enhancing the NLO properties of nitride systems and

investigates a range of UV and deep-UV NLO materials that exhibit superior linear and NLO characteristics.

Scientifically, nitride systems possess important properties that give them advantages in UV NLO materials. Firstly, wide-bandgap nitrides exhibit excellent UV transmission; for example, the optical bandgap of AlN may go as high as 6.2 eV, and its cutoff edge of UV absorption reaches 200 nm. Secondly, nitrogen has a stronger covalent nature than oxygen and is more apt to form double or triple bonds with other elements. Lastly, nitrides can form highly stable crystal structures that lend themselves to optoelectronic applications. Polar structure is a determinant of greater second-order NLO effects in nitrides compared to oxides. Additionally, nitrides can combine with oxygen or halogen to form oxygenated or halogenated nitrides with a wider range of covalent chemical bonding structures. This ultimately enables better regulation of the birefringence and endows materials with superior birefringent phase-matching properties. The wide-bandgap nitride system is highly significant for scientific research as an emerging field of exploration for UV NLO materials due to its combination of the three aforementioned advantages.

The research program in this article has three main objectives. First, we performed a systematical screening to identify polar double-bonded molecular structures, quasi-one-dimensional chained structures, and quasi-two-dimensional layered structures within known nitride material systems [24,25]. Then, to better understand the alloying properties in oxygen-nitride systems, such as $\text{Si}_2\text{N}_2\text{O}$, we could have also conducted a complete evaluation of how altering the alloying ratios affects NLO properties and ultimately improves laser output to UV 266 nm [26]. Additionally, we should further investigate the thermal stability and defect properties in selected nitride structures. Based on the defect theory of semiconductors, this study examines the properties of nitride materials when subjected to laser irradiation. The focus is on the damage caused by defects in the materials. In the course of this research program, we have discovered nitride vdW crystals (e.g., CNI) and polymeric materials (e.g., PNF_2) that exhibit excellent UV and deep-UV NLO properties. The focus of researchers now should be on developing and characterizing nitride materials with significant linear and NLO properties. The ultimate goal is to achieve the laser output at 266 nm or even at 177 nm. This objective necessitates the performance of thorough theoretical studies as well as sustained experimental exploration.

6. Conclusions

In conclusion, according to a first-principles analysis of structure–property correlations, nitride semiconductors with wide tunable energy bandgaps and abundant coordination motifs are predicted to possess potential UV NLO properties. These properties include wide UV transparency, large SHG effects, sufficient birefringence, and short phase-matching SHG output wavelengths. Regarding nitride NLO materials, our research group has previously made notable contributions to the field [24–26]. Since then, the exploration of many nitride NLO materials has flourished. This paper not only reviews these advances, but also summarizes structure–property relationships and material design options in a concise manner. As a short summary, benefits of nitride UV NLO material used include a of UV transmittance equivalent to that of oxides; superior NLO effects; increased anisotropy of the one-dimensional structure, resulting in superior phase-matching capacity; structural diversity in coordination with oxygen or halogen elements; the application of synthetic growth conditions to oxygen-free catalogs of ternary compounds, leading to the development of semiconducting properties; and material stability. Preliminary research indicates that wide-bandgap nitride materials exhibit distinct NLO characteristics across the UV to deep-UV range. Significantly, there is enhanced efficiency in the deep-UV region. This compensates for oxides' lack of deep-UV phase-matching capacity and improves overall NLO harmonic output efficiency in the deep-UV region. These advantages, although previously overlooked, make these materials potential alternatives to oxides and ensure they have a noteworthy impact on the study of inorganic NLO materials. However, a lack of theoretical understanding

has prevented systematic synthetic growth experiments. The purpose of this article relates to the use of wide-bandgap nitride semiconductors to conduct theoretical research, guide experimental exploration, develop and enrich the understanding of nitride NLO materials, and discover promising nitride UV NLO materials. Based on our research, we have found that nitrides have the potential for superior performance and advantages in UV nonlinear optics, which can help in exploring functional NLO materials in the UVC region.

Author Contributions: Conceptualization, L.K.; methodology, L.K.; software, L.K.; validation, S.L. and L.K.; formal analysis, S.L.; investigation, S.L.; resources, L.K.; data curation, S.L.; writing—original draft preparation, S.L. and L.K.; writing—review and editing, S.L. and L.K.; visualization, S.L.; supervision, L.K.; project administration, L.K.; funding acquisition, L.K. All authors have read and agreed to the published version of the manuscript.

Funding: This research was funded by National Natural Science Foundation of China (NSFC), grant number 12174404.

Acknowledgments: This work was supported by the NSFC (Grant No. 12174404).

Conflicts of Interest: The authors declare no conflict of interest. The funders had no role in the design of the study; in the collection, analyses, or interpretation of data; in the writing of the manuscript; or in the decision to publish the results.

References

1. Hao, Y.; Zhang, J.F.; Zhang, J.C. Nitride wide bandgap semiconductor material and electronic devices. *MRS Bull.* **2018**, *43*, 69.
2. Roccaforte, F.; Fiorenza, P.; Greco, G.; Lo Nigro, R.; Giannazzo, F.; Iucolano, F.; Saggio, M. Emerging trends in wide band gap semiconductors (SiC and GaN) technology for power devices. *Microelectron. Eng.* **2018**, *187–188*, 66–77. [[CrossRef](#)]
3. Liu, X.; Bruch, A.W.; Gong, Z.; Lu, J.; Surya, J.B.; Zhang, L.; Wang, J.; Yan, J.; Tang, H.X. Ultra-high-Q UV microring resonators based on a single-crystalline AlN platform. *Optica* **2018**, *5*, 1279–1282. [[CrossRef](#)]
4. Coulon, P.M.; Kusch, G.; Martin, R.W.; Shields, P.A. Deep UV emission from highly ordered AlGa_N/AlN core-shell nanorods. *ACS Appl. Mater. Interfaces* **2018**, *10*, 33441–33449. [[CrossRef](#)] [[PubMed](#)]
5. Sharma, V.; Kagdada, H.L.; Jha, P.K.; Spiewak, P.; Kurzydowski, K.J. Thermal transport properties of boron nitride based materials: A review. *Renew. Sustain. Energy Rev.* **2020**, *120*, 109622. [[CrossRef](#)]
6. Shen, D.; Shao, Y.; Zhu, Y. Bandgap trimming and optical properties of Si₃N₄: Al microbelt phosphors for warm white light-emitting diodes. *CrystEngComm* **2019**, *21*, 6566–6573. [[CrossRef](#)]
7. Chen, H.Y.; Liu, K.W.; Hu, L.F.; Al-Ghamdi, A.A.; Fang, X.S. New concept ultraviolet photodetectors. *Mater. Today* **2015**, *18*, 493–502. [[CrossRef](#)]
8. Jones-Bey, H. Deep-UV applications await improved nonlinear optics. *Laser Focus World* **1998**, *34*, 127–134.
9. Togashi, T.; Nabekawa, N.; Sekikawa, T.; Watanabe, S. Generation of milliwatt narrow-bandwidth vacuum ultraviolet radiation by an all-solid-state tunable high-average-power laser system. *Opt. Lett.* **2001**, *26*, 831–833. [[CrossRef](#)]
10. Chen, C.; Sasaki, T.; Li, R.; Wu, Y.; Lin, Z.; Mori, Y.; Hu, Z.; Wang, J.; Aka, G.; Yoshimura, M.; et al. *Nonlinear Optical Borate Crystals, Principles and Applications*; Wiley-VCH Press: Weinheim, Germany, 2012.
11. Savage, N. Ultraviolet lasers. *Nat. Photonics* **2007**, *1*, 83–85. [[CrossRef](#)]
12. Wang, X.Z.; Yuan, H.Y.; Wang, M.S.; Huang, W.C. Continuous 1052, 1064 nm dual-wavelength Nd:YAG laser. *Opt. Commun.* **2016**, *376*, 67–71. [[CrossRef](#)]
13. Zhang, X.; Wang, L.R.; Wang, X.Y.; Wang, G.L.; Zhu, Y.; Chen, C.T. High-power sixth-harmonic generation of an Nd:YAG laser with KBe₂BO₃F₂ prism-coupled devices. *Opt. Commun.* **2012**, *285*, 4519–4522. [[CrossRef](#)]
14. Eismann, U.; Scholz, M.; Paasch-Colberg, T.; Stuhler, J. Short, shorter, shortest: Diode lasers in the deep ultraviolet. *Laser Focus World* **2016**, *52*, 39–44.
15. Maker, P.D.; Savage, C.M.; Terhune, R.W.; Nisenoff, M. Effects of dispersion and focusing on production of optical harmonics. *Phys. Rev. Lett.* **1962**, *8*, 21–22. [[CrossRef](#)]
16. Giordmaine, J.A. Mixing of light beams in crystals. *Phys. Rev. Lett.* **1962**, *8*, 19–20. [[CrossRef](#)]
17. Eckardt, R.C.; Masuda, H.; Fan, Y.X.; Byer, R.L. Absolute and relative nonlinear optical coefficients of KDP, KD*P, BaB₂O₄, LiIO₃, MGO-LiNbO₃, and KTP measured by phase-matched 2nd-harmonic generation. *IEEE J. Quantum Electron.* **1990**, *26*, 922–933. [[CrossRef](#)]
18. Chen, C.T.; Wu, Y.C.; Jiang, A.D.; Wu, B.C.; You, G.M.; Li, R.K.; Lin, S.J. New nonlinear-optical crystal-LiB₃O₅. *J. Opt. Soc. Am. B* **1989**, *6*, 616–621. [[CrossRef](#)]

19. Chen, C.T.; Wu, B.C.; Jiang, A.D.; You, G.M. A new-type ultraviolet SHG crystal-beta-BaB₂O₄. *Sci. Sin. Ser. B-Chem. Biol. Agric. Med. Earth Sci.* **1985**, *28*, 235–243.
20. Chen, C.T.; Wang, G.L.; Wang, X.Y.; Xu, Z.Y. Deep-UV nonlinear optical crystal KBe₂BO₃F₂—Discovery, growth, optical properties and applications. *Appl. Phys. B* **2009**, *97*, 9–25. [[CrossRef](#)]
21. Tran, T.T.; Young, J.S.; Rondinelli, J.M.; Halasyamani, P.S. Mixed-metal carbonate fluorides as deep-ultraviolet nonlinear optical materials. *J. Am. Chem. Soc.* **2017**, *139*, 1285–1295. [[CrossRef](#)]
22. Shang, Y.; Xu, J.; Sha, H.; Wang, Z.; He, C.; Su, R.; Yang, X.; Long, X. Nonlinear optical inorganic sulfates: The improvement of the phase matching ability driven by the structural modulation. *Coord. Chem. Rev.* **2023**, *494*, 215345–215354. [[CrossRef](#)]
23. Liu, X.M.; Gong, P.F.; Yang, Y.; Song, G.M.; Lin, Z.S. Nitrate nonlinear optical crystals: A survey on structure-performance relationships. *Coord. Chem. Rev.* **2019**, *400*, 213045–213058. [[CrossRef](#)]
24. Kang, L.; Liang, F.; Lin, Z.; Liu, F.; Huang, B. Cyano-based materials with giant optical anisotropy and second harmonic-generation effect. *Inorg. Chem.* **2018**, *57*, 15001–15008. [[CrossRef](#)] [[PubMed](#)]
25. Kang, L.; Zhang, X.; Liang, F.; Lin, Z.; Huang, B. Poly(difluorophosphazene) as the first deep-ultraviolet nonlinear optical polymer: A first-principles prediction. *Angew. Chem. Int. Ed.* **2019**, *58*, 10250–10254. [[CrossRef](#)]
26. Kang, L.; He, G.; Zhang, X.; Li, J.; Lin, Z.; Huang, B. Alloy engineering of a polar (Si,Ge)₂N₂O system for controllable second harmonic performance. *Inorg. Chem.* **2021**, *60*, 7381–7388. [[CrossRef](#)] [[PubMed](#)]
27. Zhao, X.; Lin, C.S.; Chen, J.D.; Luo, M.; Xu, F.; Yang, S.D.; Shi, S.S.; Li, B.X.; Ye, N. Halonitrides Zn₂NX (X=Cl,Br): Novel mid-infrared nonlinear optical materials. *Chem. Mater.* **2021**, *33*, 1462–1470. [[CrossRef](#)]
28. Zhang, S.Z.; Kang, L.; Lin, Z.S. Nonlinear optical ASnX (A = Na, H; X = N, P) nanosheets with divalent tin lone electron pair effect by first-principles design. *Nanoscale* **2020**, *12*, 14895–14902. [[CrossRef](#)] [[PubMed](#)]
29. Kang, L.; Lin, Z.S. Second harmonic generation of MoSi₂N₄-type layers. *Phys. Rev. B* **2021**, *103*, 195404. [[CrossRef](#)]
30. Zhao, X.; Lin, C.; Tian, H.; Wang, C.; Ye, N.; Luo, M. Nitrides: A promising class of nonlinear optical material candidates. *Mater. Chem. Front.* **2023**; *advance article*. [[CrossRef](#)]
31. Jiang, X.; Kang, L.; Wang, J.F.; Huang, B. Giant bulk electrophotovoltaic effect in heteronodal-line systems. *Phys. Rev. Lett.* **2023**, *130*, 256902. [[CrossRef](#)]
32. Huang, J.; Shu, S.; Cai, G.-M. Screening nitrides with high Debye temperatures as nonlinear optical materials. *J. Phys. Chem. C* **2022**, *126*, 7047–7053. [[CrossRef](#)]
33. Huang, J.; Xie, C.; Wei, L.; Bian, Q.; Yang, Z.; Pan, S. Predicting Diamond-like nitrides as infrared nonlinear optical materials with high thermal conductivity. *Chem. Mater.* **2022**, *34*, 10059–10067. [[CrossRef](#)]
34. Chu, D.; Huang, Y.; Xie, C.; Tikhonov, E.; Kruglov, I.; Li, G.; Pan, S.; Yang, Z. Unbiased screening of novel infrared nonlinear optical materials with high thermal conductivity: Long-neglected nitrides and popular chalcogenides. *Angew. Chem. Int. Ed.* **2023**, *62*, e202300581. [[CrossRef](#)] [[PubMed](#)]
35. Kang, L.; Liang, F.; Jiang, X.; Lin, Z.; Chen, C. First-principles design and simulations promote the development of nonlinear optical crystals. *Acc. Chem. Res.* **2019**, *53*, 209–217. [[CrossRef](#)] [[PubMed](#)]
36. Chen, C.; Lin, Z.; Wang, Z. The development of new borate-based UV nonlinear optical crystals. *Appl. Phys. B Lasers Opt.* **2005**, *80*, 1–25. [[CrossRef](#)]
37. Liu, X.; Kang, L.; Lin, Z. Regulating guanidinium-based hybrid materials for ultraviolet nonlinear optical applications by hybrid strength and hybrid pattern. *Inorg. Chem.* **2021**, *60*, 3834–3842. [[CrossRef](#)] [[PubMed](#)]
38. Kakanakova-Georgieva, A.; Ivanov, I.G.; Suwannaharn, N.; Hsu, C.-W.; Cora, I.; Pécz, B.; Giannazzo, F.; Sangiovanni, D.G.; Gueorguiev, G.K. MOCVD of AlN on epitaxial graphene at extreme temperatures. *CrystEngComm* **2021**, *23*, 385–390. [[CrossRef](#)]
39. Kakanakova-Georgieva, A.; Nilsson, D.; Stattin, M.; Forsberg, U.; Haglund, Å.; Larsson, A.; Janzén, E. Mg-doped Al_{0.85}Ga_{0.15}N layers grown by hot-wall MOCVD with low resistivity at room temperature. *Phys. Status Solidi RRL* **2010**, *4*, 311–313. [[CrossRef](#)]
40. Kang, L.; Lin, Z. Deep-ultraviolet nonlinear optical crystals: Concept development and materials discovery. *Light-Sci. Appl.* **2022**, *11*, 201. [[CrossRef](#)]
41. Hao, X.; Luo, M.; Lin, C.S.; Peng, G.; Xu, F.; Ye, N. M(NH₂SO₃)₂ (M=Sr, Ba): Two deep-ultraviolet transparent sulfamates exhibiting strong second harmonic generation responses and moderate birefringence. *Angew. Chem. Int. Ed.* **2021**, *60*, 7621–7625. [[CrossRef](#)]
42. Cruickshank, D.W.J. Refinements of structures containing bonds between Si, P, S or Cl and O or N.I. NaPO₃NH₃. *Acta Crystallogr.* **1964**, *17*, 671–672. [[CrossRef](#)]
43. Alves Machado Filho, M.; Hsiao, C.-L.; dos Santos, R.B.; Hultman, L.; Birch, J.; Gueorguiev, G.K. Self-Induced Core-Shell InAlN Nanorods: Formation and Stability Unraveled by Ab Initio Simulations. *ACS Nanosci. Au* **2023**, *3*, 84–93. [[CrossRef](#)] [[PubMed](#)]
44. Talley, K.R.; Perkins, C.L.; Diercks, D.R.; Brennecka, G.L.; Zakutayev, A. Synthesis of LaWN₃ nitride perovskite with polar symmetry. *Science* **2021**, *374*, 1488–1491. [[CrossRef](#)] [[PubMed](#)]
45. Zhao, H.J.; Chen, P.; Paillard, C.; Arras, R.; Fang, Y.-W.; Li, X.; Gosteau, J.; Yang, Y.; Bellaiche, L. Large spin splittings due to the orbital degree of freedom and spin textures in a ferroelectric nitride perovskite. *Phys. Rev. B* **2020**, *102*, 041203. [[CrossRef](#)]
46. Fichtner, S.; Wolff, N.; Lofink, F.; Kienle, L.; Wagner, B. AlScN: A III-V semiconductor based ferroelectric. *J. Appl. Phys.* **2019**, *125*, 114103. [[CrossRef](#)]

47. Jena, D.; Page, R.; Casamento, J.; Dang, P.; Singhal, J.; Zhang, Z.; Wright, J.; Khalsa, G.; Cho, Y.; Xing, H.G. The new nitrides: Layered, ferroelectric, magnetic, metallic and superconducting nitrides to boost the GaN photonics and electronics eco-system. *Jpn. J. Appl. Phys.* **2019**, *58*, SC0801. [[CrossRef](#)]
48. Sun, W.; Bartel, C.J.; Arca, E.; Bauers, S.R.; Matthews, B.; Orvañanos, B.; Chen, B.R.; Toney, M.F.; Schelhas, L.T.; Tumas, W.; et al. A map of the inorganic ternary metal nitrides. *Nat. Mater.* **2019**, *18*, 732–739. [[CrossRef](#)]

Disclaimer/Publisher’s Note: The statements, opinions and data contained in all publications are solely those of the individual author(s) and contributor(s) and not of MDPI and/or the editor(s). MDPI and/or the editor(s) disclaim responsibility for any injury to people or property resulting from any ideas, methods, instructions or products referred to in the content.